A quasi-distributed dynamic and static strain sensor system*

JING Wen-cai, LIU Tao, ZHANG Pei-song, LIU Kun, JIA Da-gong, and ZHANG Yi-mo**

College of Precision Instrument & Optoelectronics Engineering, Key Laboratory for Optoelectronic Information and Technical Science of Ministry of Education, Tianjin Universiey, Tianjin 300072, China

(Received 21 January 2008)

A quasi-distributed dynamic and static strain sensor system consisting of 16 FBG sensors is designed by using an amplified-sponteneous emission (ASE) optical source, an optical tunable filter and a tunable laser. A resolution of about 5 με has been achieved for dynamic strain measurement. The resolution for static strain measurement is about 1 με.

CLC numbers: TN253 **Document code:** A **Article ID:** 1673-1905(2008)04-0243-5

DOI 10.1007/s11801-008-8014-6

Fibre Bragg gratings (FBGs) are increasingly used as strain sensors in the monitoring of large-scale concrete structures [1-3]. They provide real-time strain sensing and can be either embedded into the structure, or attached to the surface. Compared with mechanical sensors, they are light, compact, immune to electro-magnetic interference, easy to be installed, and can be easily multiplexed in a large-scale distributed strain monitoring network [4]. Many methods have been studied for monitoring strain and temperature simultaneously, including the use of fibre Bragg grating cavity, Fabry-Perot cavity, tilted fibre Bragg grating, chirped Bragg grating, sampled fibre Bragg grating, Brillion reflection, dual-gratings [5-10],and etc.

In this research, a FBG sensor is used as a temperature sensor to compensate the thermal influence at other sensors. An ASE source and optical tunable filter are used to monitor the dynamic strain at a sample rate of up to 6 samples per second. The strain resolution is about 5 με at a sample rate of 2 samples per second. A tunable laser is used to monitor the long-term strain drift. A strain resolution of 1 ìå is achieved for the static strain measurement. The influence of electronic circuit noise, optical noise, sampling rate, wavelength scanning step, tunable filter nonlinearity and signal processing algorithms are also discussed in this paper.

The Bragg wavelength of a grating is given by

$$\lambda_B = 2n\Lambda \ , \tag{1}$$

where Λ is the grating pitch and n is the reflective index of the grating core. The change of the Bragg wavelength can be calculated as follows[11]:

$$\Delta\lambda_B = \frac{\partial\lambda_B}{\partial\varepsilon}\Delta\varepsilon + \frac{\partial\lambda_B}{\partial T}\Delta T, \tag{2}$$

where $\Delta\varepsilon$ is the applied longitudinal strain and ΔT is the change of environmental temperature. The strain coefficient of the Bragg wavelength shift can be calculated as follows:

$$\frac{\partial\lambda_B}{\partial\varepsilon} = 0.78\times10^{-6}\cdot\lambda_B \ . \tag{3}$$

The thermal coefficient can be expressed by using

$$\frac{\partial\lambda_B}{\partial T} = 7.02\times10^{-6}\cdot\lambda_B \ . \tag{4}$$

The structure of the quasi-distributed dynamic and static sensor system is shown in Fig.1. It consists of two parts, i.e. the dynamic strain measurement subsystem and the static strain measurement subsystem. The sensors are divided into two groups, group one and group two. Each group has eight sensors, labeled S_{11} to S_{18} and S_{21} to S_{28}, respectively. The dynamic strain measurement subsystem uses an ASE source and an optical tunable filter to interrogate the Bragg wavelength shift. A 16-bit Labview card is adopted to generate the sawtooth wave, which is used to drive the optical tunable filter after amplification. The filtered optical signal is converted to an electrical signal at the photodetector, and then sampled via the analogue to digital channel of the Labview card for further processing. The dynamic strain measurement

* This work has been supported by the National Natural Science Foundation of China (No.60377031), the National Basic Research Program of China (No.2003CB314907), and the Program for New Century Excellent Talents in University.

** E-mail:tjuliutao@yahoo.com.cn.

subsystem can only detect the wavelength shift of the sensors. It cannot detect the absolute wavelength, because the optical tunable filter itself can be only used to detect the wavelength difference rather than the absolute wavelength. The static strain measurement subsystem uses a tunable laser and a photodetector to interrogate the wavelength shift of the sensors. It can detect the absolute wavelength of the sensors. So this subsystem can be used to monitor the long-term shift of the Bragg wavelength. As a result, it can be used to detect the long-term strain drift of the construction.

The dynamic strain measurement subsystem can sample the strain at each sensor at a rate of up to 6 samples per second. While the sampling rate of the static strain measurement subsystem is only 2 samples per minute, which is limited by the tuning speed of the tunable laser.

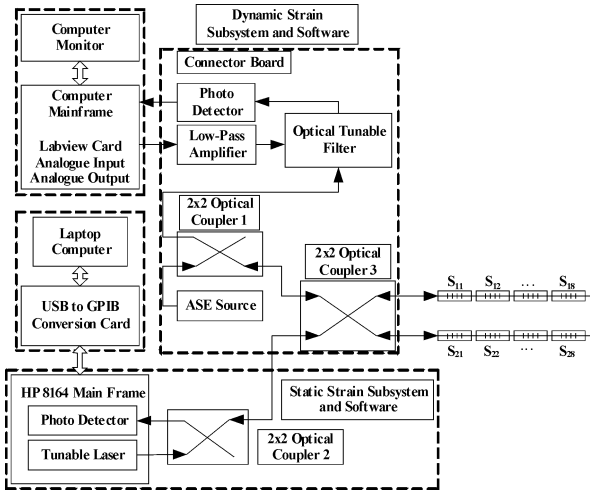

Fig.1 The structure of the quasi-distributed dynamic and static sensor system

Both the static strain and the dynamic strain measurement subsystems can work individually, without reference to the other subsystem. On the other hand, they can work together as a whole system to eliminate the limitation of an individual subsystem. Generally speaking, the static subsystem can work periodically, at an interval from several minutes to a few hours or even longer. Meanwhile, the dynamic subsystem needs to work continuously to monitor the real-time strain of the construction. So the performance of the static subsystem depends on the long-term wavelength stability of the tunable laser. At the same time, the performance of the dynamic subsystem depends on the time-response of the electrical and optical devices, as well as the spectrum resolution of the optical tunable filter.

A typical measurement result of the static strain subsystem is shown in Fig. 2. It shows the measured strain at two sensors over a time span of more than two hours. During that time, an environmental temperature fluctuation of about 1.2 °C is observed by using a conventional temperature sensor. One of the FBG sensors is used as a temperature sensor to compensate the thermal influence. The difference between the FBG temperature sensor and the conventional temperature sensor is less than 0.1 °C. After temperature compensation, the strain deviation at each sensor is less than 1 με. During the strain measurement period, a constant strain is applied at each sensor. The strain fluctuation is mainly caused by changing the environment temperature. Since the distance between each strain sensor and the temperature sensor is different, there is a temperature difference between the two strain sensors. As a result, the thermal influence is not completely compensated. Each sensor shows a slow drift of the strain, which is caused by the residual thermal effect.

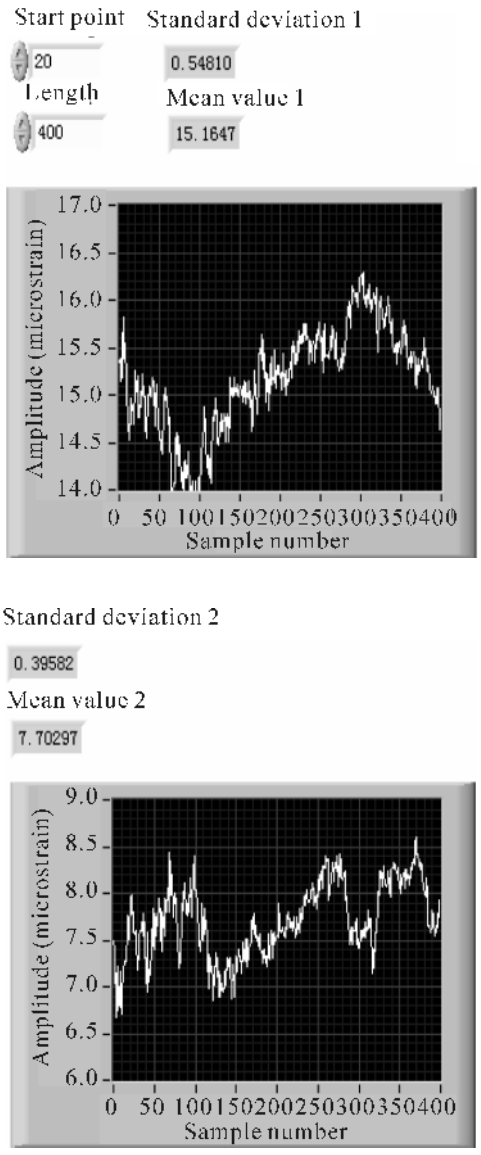

Fig.2 Static strain measurement results

To further reduce the thermal effect, a possible method is to use two FBG sensors as a subgroup, with one FBG used as a temperature sensor and the other as a strain sensor. Meanwhile, the two FBGs are mounted in each subgroup as close as possible to reduce the thermal effects. The disadvantage of this method is the increase of the FBG number, and the decreases of the strain measurement points in the network at a certain given wavelength tuning range of the tunable laser and a minimum wavelength gap between two adjacent spectrums of the FBGs.

The experimental results of the dynamic strain measurement subsystem are shown in Tab.1.

Tab.1 The tested results of the dynamic strain measurement subsystem

Sensor No.	S11	S12	S13	S14	S15	S16	S17	S18
Wavelength (nm)	1541.33	1537.17	1538.10	1538.97	1540.26	1526.84	1528.56	1529.63
Standard deviation ($\mu\varepsilon$)	2.6	2.1	2.4	2.3	2.5	Reference sensor	1.6	1.4
Sensor No.	S21	S22	S23	S24	S25	S26	S27	S28
Wavelength (nm)	1565.05	1564.33	1562.64	1558.02	1556.67	1533.73	1545.50	1551.25
Standard deviation($\mu\varepsilon$)	5.8	6.3	5.6	4.4	4.7	2.0	3.3	3.7

In both the static and dynamic strain measurement subsystems, the interrogation of strain is directly correlated to the measurement of the Bragg wavelength shift of the sensors. As each sensor has a full width half maximum (FWHM) spectrum width, the test results are dependent on the algorithms used to calculate the characteristic wavelength (CW) of each sensor. In this work, three algorithms are adopted to calculate the CW of each sensor, namely the peak intensity detection (PID), the weighted centre wavelength (WCW) [12] and the linear fit (LF) [13].

PID algorithm is the simplest one to calculate the CW of each sensor. It detects the peak value in each sensor spectrum. The wavelength corresponding to the peak value is defined as the CW of the sensor. Due to the sampling error and the system noise, this algorithm leads to the largest measurement error among the three algorithms. Meanwhile, this algorithm is sensitive to the wavelength-sampling steps. The relationship between the standard deviation of the measured strain and the wavelength step is shown in Fig. 3. For ease of display, this figure only incorporates the results of three sensors, with each sensor indicating similar changing trend. It is obvious that this algorithm is sensitive to the wavelength steps.

In this algorithm, the CW of each sensor is calculated as follows:

$$\lambda_{CW}=\sum\lambda_i P_i/\sum P_i \quad , \tag{5}$$

where λ_i is the wavelength sample of the sensor spectrum, and P_i is the intensity of the spectrum at λ_i. The wavelength-sampling step and the numbers of data-points, i.e. the wavelength windows, affect the measurement resolution of this algorithm. When the wavelength window is larger than 600 pm, the standard deviation calculated by using the algorithm is not sensitive to the wavelength-sampling steps under 70 pm, see Fig.4.

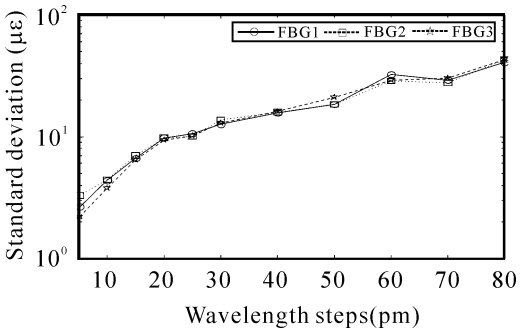

Fig.3 The relationship between the standard deviation of measured strain and the the wavelength steps by using PID algorithm

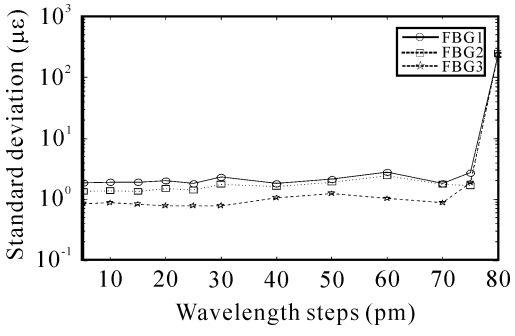

Fig.4 The relationship between the standard deviation of measured strain and the wavelength steps by using WCW algorithm

In this algorithm a set of data points on the falling edge of each sensor spectrum is used to fit a straight line and to calculate the wavelength on the line that corresponds to half maximum on the spectrum. Fig.5 illustrates how the CW is calculated by using this algorithm. The standard deviation calculated by using the algorithm is not sensitive to the wavelength-sampling steps under 90 pm, see Fig.6.

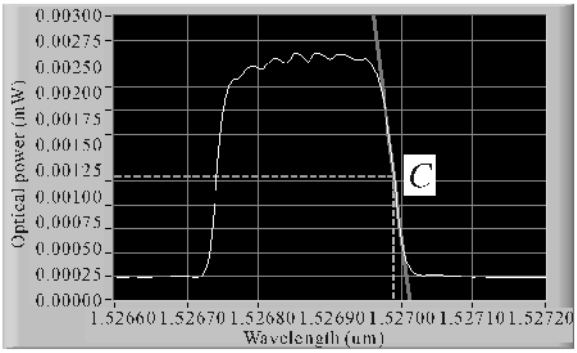

Fig.5 Calculation result of the CW with LF algorithm

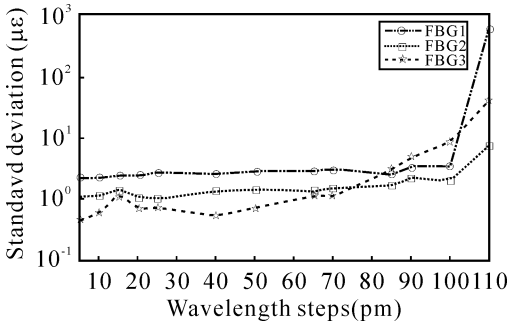

Fig.6 The relationship between the standard deviation of measured strain and the wavelength steps with LF algorithm

System noise and sampling rate of the electronic circuits also affect the system performance. System noise is caused by the optical source fluctuation, background light, photodetector noise, analogue to digital conversion (ADC) digitization error and other circuit noise. In this system, the ADC digitization error is dominant when the digital outputs are 12 bits or less. When the ADC digital output is 16 bits, the background light becomes the dominant factor.

For the dynamic strain measurement, the time response of the system is another key issue to be considered. The maximum strain-sampling rate under a certain resolution is mainly determined by the data-sampling frequency of the ADC circuits, software overheads, and time response of the optical tunable filter. In this system, software overheads and ADC circuits sampling frequency are the dominant factors. During strain measurement process, a lot of data need to be processed in real time and logged to a hard disk. Significant reduction in the strain-sampling rate has been observed in the measurement compared with the situation where no data-logging is performed. Fig.7 shows the influence of strain-sampling rate on the measurement results.

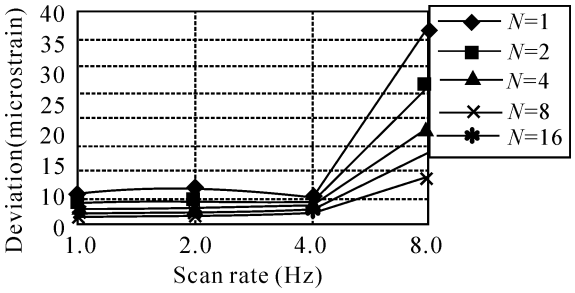

Fig.7 Relationship between the standard deviation of measured strain and sampling rate

There is a significant increase of the standard deviation of measured stain when the sampling rate is increased from 4 Hz to 8 Hz. The parameter *N* in this figure is the number of data points used in moving average for data processing. This parameter also affects time response of the dynamic strain measurement subsystem.

A quasi-distributed dynamic and static strain sensor system consisting of 16 FBG sensors is designed by using an ASE optical source, an optical tunable filter, and a tunable laser. A resolution of about 5 iå has been achieved for dynamic strain measurement at two strain samples per second per sensor. The resolution for static strain measurement is about 1 με. The influence of electronic circuit noise, optical noise, sampling rate, wavelength scanning steps, tunable filter nonlinearity and signal processing algorithms have been also discussed.

References

[1] Allan D. Kersey, Michael A. Davis, Heather J. Patrick, Journal of Lightwave Technology, **15** (1997), 1442.

[2] Sean Calvert, and Jason Mooney, Smart Strunctures ans Materials 2004: Sensors and Smart Structures Technologies for Civil, Mechanical, and Aerospace Systems, Shih-Chi Liu Ed., Proc. Of SPIE, **5391** (2004), 61.

[3] S. W. James, M. L. Dockney, and R. P. Tatam, Electron. Lett., **32** (1996), 1133.

[4] Yumei Fu, Yong Zhu, Weimin Chen, et al, Smart Strunctures ans Materials 2004: Sensors and Smart Structures Technologies for Civil, Mechanical, and Aerospace Systems, Shih-Chi Liu Ed., Proc. Of SPIE, **5391** (2004), 732.

[5] M. C. Golt, A. F. Lipiecki, A. P. Schmalz, Smart Strunctures ans Materials 2004: Sensors and Smart Structures Technologies for Civil, Mechanical, and Aerospace Systems, Shih-Chi Liu Ed., Proc. Of SPIE, **5391** (2004), 741.

[6] A. T. Alavie, S. E. Karr, A. Othonos, and R. M. Measures, IEEE Photonics Technol. Lett., **5** (1993), 1112.

[7] Bai-Ou Guan, Hwa-Yaw Tam, and Siu-Lau Ho, Electron. Lett., **36** (2000), 1018.

[8] Wei-Chong Du, Xiao-Ming Tao, and Hwa-Yaw Tam, IEEE Photonics Technol. Lett., **11** (1999), 105.

[9] O. Frazao, R. Romero, and G. Rego, Electron. Lett., **38** (2002), 693.

[10] Bai-Ou Guan, Hwa-Yaw Tam, and Xiao-Ming Tao, IEEE Photonics Technol. Lett., **12** (2000), 675.

[11] Jianjun Ma, Weizhong Tang, and Wen Zhou, Applied Optics, **35** (1996), 5206.

[12] Jing Wen-cai, Wang Guang-hui, and Liu Kun, Optoelectronics • Laser, **18** (2007), 1022 (in Chinese).

[13] Dong Hai, Jing Wencai, and Liu Kun, Optoelectronics • Laser, **18** (2007), 144 (in Chinese).